

# **Electrokinetic Biosensing at Liquid-Liquid Interfaces**

by

Nicholas Mavrogiannis

A thesis submitted to Johns Hopkins University in conformity with the requirements for the  
degree of Master of Science in Engineering

Baltimore, Maryland

August, 2014

© 2014 Nicholas Mavrogiannis  
All Rights Reserved

# Abstract

Development of low-cost, rapid, sensitive and portable biosensing systems are important for the detection and prevention of disease in developing countries, biowarfare/anti-terrorism applications, environmental monitoring, point-of-care diagnostic testing and for basic biological research. Currently, the most established commercially available and widespread assays for portable point of care detection and disease testing are paper-based dipstick and lateral flow test strips. These paper-based devices are often small, cheap and simple to operate. The last three decades in particular have seen an emergence of these assays in diagnostic settings for the detection of pregnancy, HIV/AIDS, blood glucose, Influenza, urinary protein, cardiovascular disease, respiratory infections and blood chemistries. Such assays are widely available largely because they are inexpensive, lightweight, portable, are simple to operate, and a few platforms are capable of multiplexed detection for a small number of sample targets.

In this paper, we present, in three parts, the first non-optical technique for detecting and quantifying chemical and biomolecular reactions in solution phase. First, an interfacial tilt is explored utilizing Maxwell-Wagner (MW) stress. Two fluids of varying electrochemical properties, conductivity and permittivity, are forced to flow side by side. When an electric field is applied across the interface a liquid displacement occurs across the interface. This displacement is found to be frequency dependent. At low frequency, roughly 1 MHz, the fluid with a higher conductivity displaces into that of a lower conductivity. On the contrary, at high frequencies, roughly 20 MHz, the fluid with the high permittivity displaces into the fluid with a lower permittivity. The frequency in which no displacement occurs is known as the crossover frequency (COF). Next, for ion and biodetection, the interface created between these two streams

is comprised of one liquid containing the analyte of interest and a second liquid containing a receptor. Analyte-receptor binding at the interface changes the interfacial electrical polarizability, and this change in polarizability can be detected by measuring the physical interfacial “tilt” during exposure to the AC electric field. The frequency-dependence of this displacement is highly sensitive to receptor:ligand binding at the interface, and by measuring this displacement as a function of frequency, the presence of an analyte can be determined. When a reaction occurs downstream the channel, the COF of the system increases, yet when no reaction occurs, the COF decreases down the channel, due to diffusion.

Advisor: Dr. Zachary Gagnon

Reader: Dr. Joelle Frechette

# Acknowledgments

Thank you to my family, friends, and Professor Gagnon

# Table of Contents

<b>Abstract</b>	<b>ii</b>
<b>Acknowledgments</b>	<b>iv</b>
<b>Table of Contents</b>	<b>v</b>
<b>List of Figures</b>	<b>vi</b>
<b>Chapter 1</b>	<b>1</b>
<b>Introduction</b>	<b>1</b>
<b>Chapter 2</b>	<b>5</b>
<b>Materials and Methods</b>	<b>5</b>
2.1 Microfluidic Device Fabrication	5
2.2 Chemical Solutions	10
2.3 Pressure System	11
2.4 Construction of a Microfluidic Liquid/Liquid Interface	13
<b>Chapter 3</b>	<b>15</b>
<b>Background</b>	<b>15</b>
3.1 Maxwell-Wagner Polarization at Liquid-Liquid Interfaces	15
3.2 Calcium Green-1	17
3.3 Biotin and Avidin	18
<b>Chapter 4</b>	<b>20</b>
<b>Results and Discussion</b>	<b>20</b>
4.1 Fluidic Dielectrophoresis	20
4.2 Calcium Detection	23
4.3 Avidin-Biotin Reaction	28
<b>Chapter 5</b>	<b>32</b>
<b>Conclusion and Future Work</b>	<b>32</b>

# List of Figures

Figure 1	Master Mold and PDMS Fabrication	6
Figure 2	Metal Deposition and Electrode Fabrication	7
Figure 3	Photomask Illustrating the Electrode Design	8
Figure 4	Brightfield image of the inlet of the microfluidic T-channel with embedded electrodes	9
Figure 5	Microfluidic T channel with embedded electrodes. Two fluid streams with different electrical properties— each imaged with a fluorescent dye—flow side by side to create an electrical interface.	10
Figure 6	Custom pressure system utilized for delivering samples to the microfluidic device	12
Figure 7	Rigol DG 4102 Function Generator used to deliver an electric field with varying frequencies and voltages across the liquid-liquid interface	13
Figure 8	Illustration of frequency-dependent MW polarization.	16
Figure 9	Calcium Green-1 Structure	18
Figure 10	Biotin Structure	18
Figure 11	Confocal cross section of the interface	21
Figure 12	Figure 10. Comparison between experimental (symbols) and analytical (line) interfacial COF as a function of the difference in electrical conductivity between each fluid stream, $[\sigma_1 - \sigma_2]$ . Error bars are of the order of the size of symbols.	23

Figure 13	Comparison between experimental (symbols) and analytical (line) interfacial COF as a function of the difference in electrical conductivity between each fluid stream, $[\varepsilon_1 - \varepsilon_2]$ . Error bars are of the order of the size of symbols.	23
Figure 14	Microfluidic T-channel zoomed in on the interface	24
Figure 15	Confocal cross section of the interface. Reaction between CG1 and $\text{Ca}^{2+}$ occurring at the interface	25
Figure 16	Comparison between experimental (symbol) and theoretical (line) COF down the axial length of the channel	27
Figure 17	Calculated COF down the axial length of the channel for CG1, Dextran (positive control), and KCl (negative control)	29
Figure 18	Calculated COF down the axial length of the channel for Biotin-Avidin, Avidin-AHA (control), and Biotin-Buffer A (control)	
Figure 19	Calculated COF down the axial length of the channel at varying flowrates	

# Chapter 1

## Introduction

Development of low-cost, rapid, sensitive and portable biosensing systems are important for the detection and prevention of disease in developing countries, biowarfare/anti-terrorism applications, environmental monitoring, point-of-care diagnostic testing and for basic biological research. Currently, the most established commercially available and widespread assays for portable point of care detection and disease testing are paper-based dipstick and lateral flow test strips. These paper-based devices are often small, cheap and simple to operate. The last three decades in particular have seen an emergence of these assays in diagnostic settings for the detection of pregnancy, HIV/AIDS, blood glucose, Influenza, urinary protein, cardiovascular disease, respiratory infections and blood chemistries. Such assays are widely available largely because they are inexpensive, lightweight, portable, are simple to operate, and a few platforms are capable of multiplexed detection for a small number of sample targets.

However, there is a critical need for sensitive, quantitative and multiplexed detection capabilities for point-of-care diagnostics and for the detection and prevention of disease in the developing world that cannot be satisfied by current state-of-the-art paper-based assays. For example, applications including the detection of cardiac and cancer biomarkers and biothreat applications require sensitive multiplexed detection of analytes in the nM and pM range, and cannot currently be satisfied with current inexpensive portable platforms due to their lack of sensitivity, quantitative capabilities and often unreliable performance.

Traditionally, biomolecular applications are focused on the detection of specific nucleotide sequences within a pathogen genome or the detection of biomarker-specific proteins as markers for disease or human health. Biosensors typically integrate two basic components for



successful operation: a biological sensing element which is a specific biomolecular interaction, such as an antibody that binds to a target protein, and a signal transducer, which converts this targeted binding event into a measurable signal. In biosensors, the bioreceptor is designed to interact with an analyte of interest, thereby producing a response, which the transducer measures. Common recognition elements include, antibody/antigen<sup>1</sup>, enzymes<sup>2</sup>, nucleic acids/DNA<sup>3</sup>, and cellular structures/cells<sup>4</sup>. The other component by which biosensors are characterized is the transducer, which can be electrochemical<sup>5</sup>, optical<sup>6</sup>, calorimetric<sup>7</sup>, or acoustic<sup>8</sup>.

One of the most popular biosensing approaches includes optical-based techniques. These methods commonly require fluorescence and the fluorescent tagging of biomolecular target probes. Although optical-sensitive molecular detection techniques provide sensitive and specific detection of a target analyte in a sample and often possess multiplexing capabilities, the majority of these techniques pose great challenges in terms of development into simple to operate, portable, sensitive and inexpensive biosensing platforms. First, these methods commonly rely on the costly and time consuming chemical conjugation of biorecognition molecules to either enzymes or fluorescent probes for optical detection. Second, periodic rinsing steps are often required in order to avoid non-specific binding, biofouling, and to remove non-binding probes from functionalized array substrates. Finally, optical methods are often limited to laboratory settings, since fluorescent detection instrumentation is often required to detect surface binding events and is still too bulky and costly for widespread daily, clinical and portable point-of-care use. Several label-free optical techniques include SPR<sup>9</sup> and Raman spectroscopy<sup>10</sup> have been applied to optically detect and measure reaction kinetics of biomolecules, however, these approaches are costly and lack portability.

The ideal biosensing platform with the ultimate attractiveness for both portable point of care use and commercialization potential is an inexpensive system, which can go from sample loading to facile biomolecular detection in a single step without the need for external supporting equipment. These types of systems are especially needed in the developing world where inhabitants lack access to basic technical services and human resources. The biosensing platform proposed here will satisfy this ultimate goal, as well as overcome the challenges facing the application of diagnostics in resource-poor settings: **(i)** affordable, **(ii)** sensitive, **(iii)** specific, **(iv)** user-friendly, **(v)** rapid and robust, **(vi)** equipment-free and **(vii)** delivered to those who need it, or “ASSURED” for short, as required by the World Health Organization (WHO).<sup>11</sup>

A major obstacle to the development of a robust, inexpensive, sensitive and portable biosensing platform with multiplexing capability is the lack of an available biosensor that is rapid, and specific to small concentrations of target biomolecules yet still capable of (1) being integrated inexpensively into miniaturized diagnostics systems, (2) does not require the labeling of probes or optical microscopy and (3) can operate without the need for complex and bulky supporting instrumentation.

This paper presents, in three parts, the first non-optical technique for detecting and quantifying chemical and biomolecular reactions in solution phase. First, an interfacial tilt is explored utilizing Maxwell-Wagner (MW) stress.<sup>12</sup> Two fluids of varying electrochemical properties, conductivity and permittivity, are forced to flow side by side. When an electric field is applied across the interface a liquid displacement occurs across the interface. This displacement is found to be frequency dependent. The frequency in which no displacement occurs is known as the crossover frequency (COF). Depicted in Figure 5, the interface created between these two streams is comprised of one liquid containing the analyte of interest and a

second liquid containing a receptor. Analyte-receptor binding at the interface changes the interfacial electrical polarizability, and this change in polarizability can be detected by measuring the physical interfacial “tilt” during exposure to the AC electric field. The frequency-dependence of this displacement is highly sensitive to receptor:ligand binding at the interface, and by measuring this displacement as a function of frequency, the presence and amount of an analyte can be determined.

Electrokinetic detection was accomplished for two different systems: chemical detection of calcium ions, and the biodetection of avidin:biotin binding.

# Chapter 2

## Materials and Methods

### 2.1 Microfluidic Device Fabrication

The microfluidic “T-channel” device was fabricated using standard soft photolithography and microfabrication techniques.

#### *2.1.1 Master Mold Fabrication*

A master mold was fabricated on a silica wafer using a negative photoresist. First the photoresist (SU-8 3050) was spin coated to 60  $\mu\text{m}$  thickness. The wafer was then softbaked at 65 °C and pre-exposure baked at 95 °C before exposure. A transparency mask was then aligned and the wafer was UV exposed. The wafer was then post-exposure baked at 95 °C before developing in SU-8 developer. After the wafer was developed it was hardbaked at 200 °C in order to smooth out the features. A 10:1 mixture of PDMS elastomer and curing agent was poured atop the wafer and baked at 85°C for 30 minutes. The PDMS was gently peeled off the wafer and the design is cut out of the mold. Fluid ports were punched with a .75 mm diameter biopsy punch (Ted Pella, Inc.).

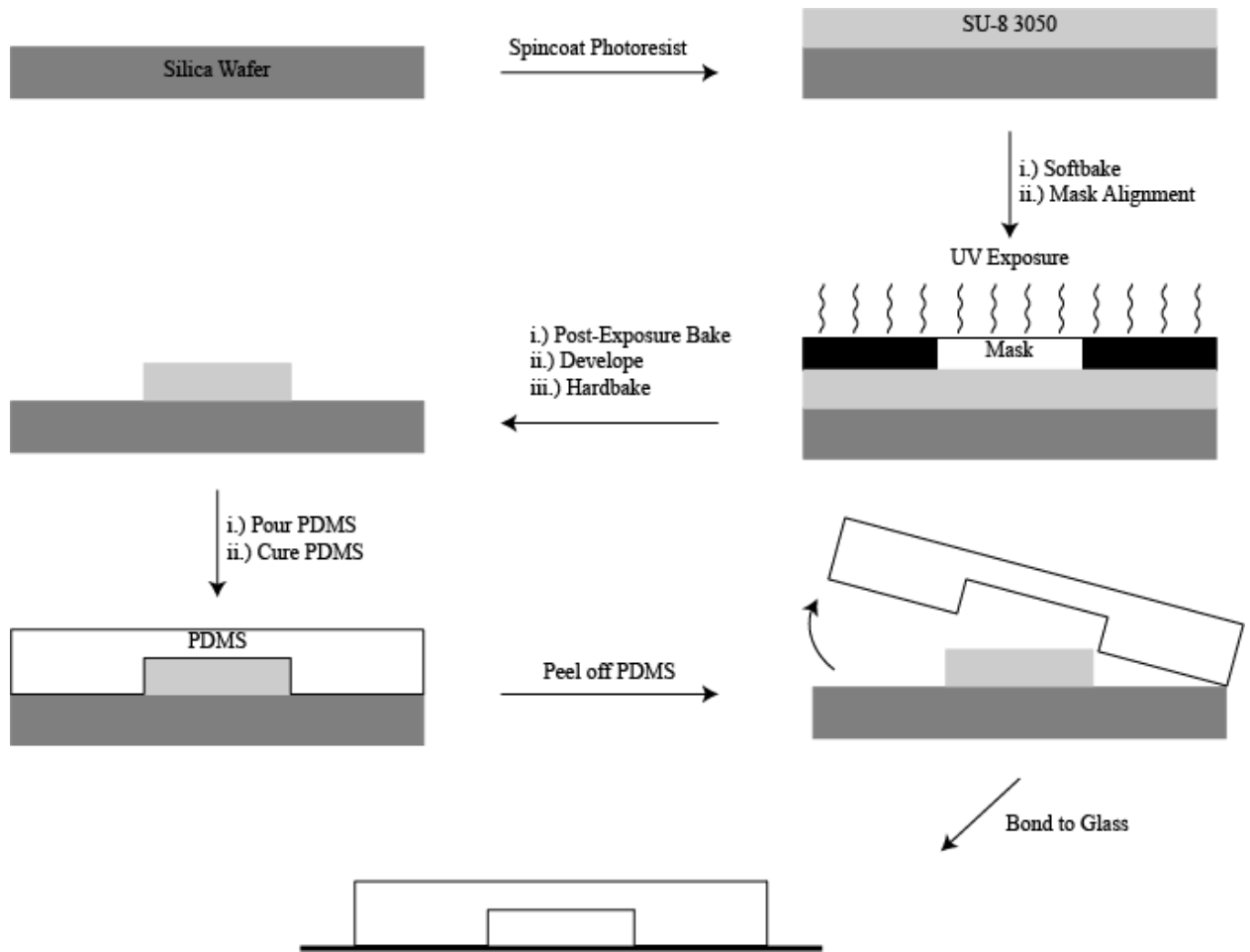


**Figure 1. Master mold and PDMS fabrication**

### **2.1.2 Electrode Fabrication**

Microchannel electrodes were fabricated using wet chemical etching techniques. Glass cover slips (50x30 mm, no.1, Fisher Scientific) were coated with 2nm of chromium and 50 nm of gold using electron beam evaporation. Electron beam deposition is a form of vapor deposition in which a target anode is bombarded with electrons. The target metal, or the source, sublimates and transforms into the gaseous phase. The atoms then precipitate into solid form, coating everything in the chamber, specifically the target substrate, glass coverslips in this case. When depositing gold onto glass substrates a second metal is needed, this metal is known as the adhesive layer.

Gold alone cannot adhere to glass, yet it can adhere to another metal such as chromium. Since chromium can adhere to glass alone, it is used as an adhesion layer for gold attachment. Once gold-coated coverslips have been fabricated, they can be patterned to create electrodes. The entire process from deposition to patterning is illustrated in Figure 2. below,

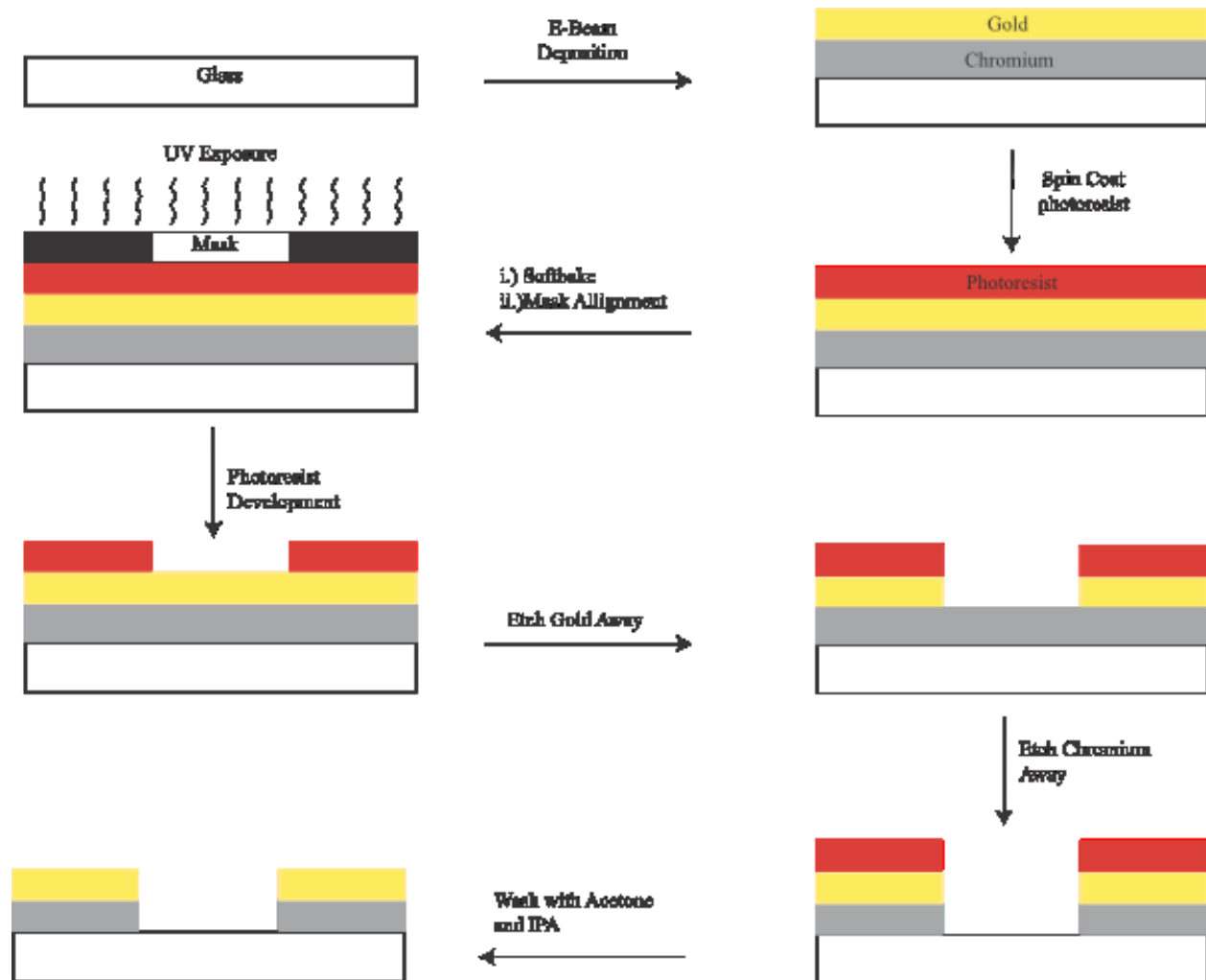


**Figure 2. Metal deposition and electrode fabrication**

The cover slips were patterned with photoresist (Shipley 1813) and exposed metal was etched using gold and chromium etchant. First the photoresist was spin coated onto the gold coverslips

with a 1.5  $\mu\text{m}$  thickness. The slides were then baked at 95  $^{\circ}\text{C}$  for 2 minutes. Once the slides cooled, a mask aligner was used to align a photomask, shown in Figure 3., with the slide.

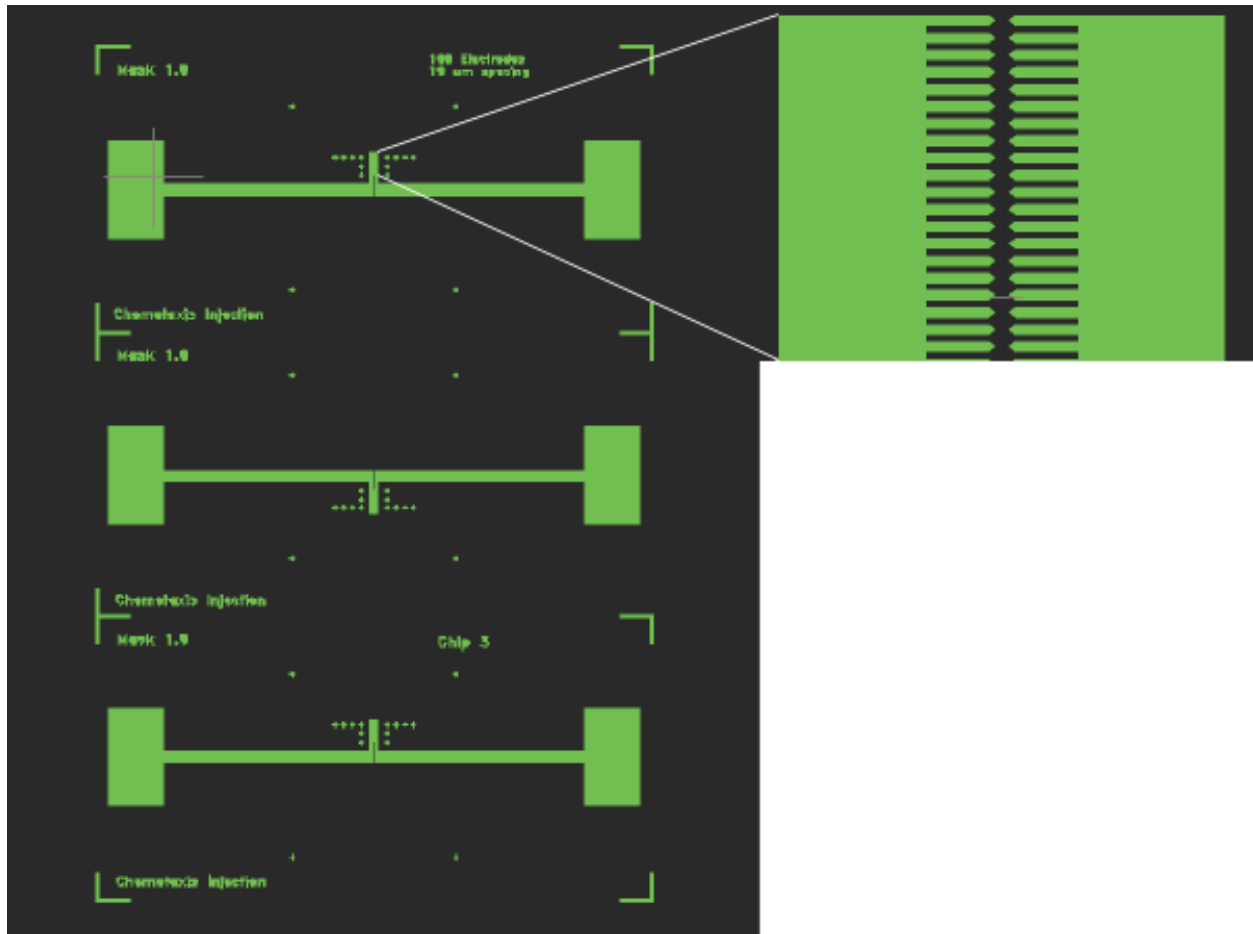


**Figure 3. Photomask illustrating the electrode design**

Since the photoresist is a positive photoresist, any portion of the photoresist that is exposed to UV light will cure and remain on the slide during development. Once the slide was UV exposed it was developed in MF-26 developer for 2 minutes and washed with DI water. Once the pattern was suitable for etching the slide was submerged in gold etchant for 10 seconds, then chromium etchant for 1 minute. The slide was then washed with acetone to remove left-behind photoresist, and isopropanol to remove acetone.

### **2.1.3 Bonding**

The resulting electrode pattern was aligned and bonded to a soft lithographically fabricated polymer “T-channel” design. The electrode-patterned coverslip was then exposed to oxygen plasma (Jelight, Model 42A) and the PDMS microchannel was exposed using a handheld tesla coil (Vendor ID). The two substrates were then immediately aligned and sealed under an inverted microscope. As shown in Figure 4., the device consists of a main flow channel 100  $\mu\text{m}$  wide and 65  $\mu\text{m}$  high. The embedded electrodes are axially separated by 20  $\mu\text{m}$  and symmetrically bridge the channel width. Here, electrodes with sharp points are utilized in order to maximize the electric field strength across the liquid interface, as the sharp point serves to focus the electric field to the tip of the electrode.

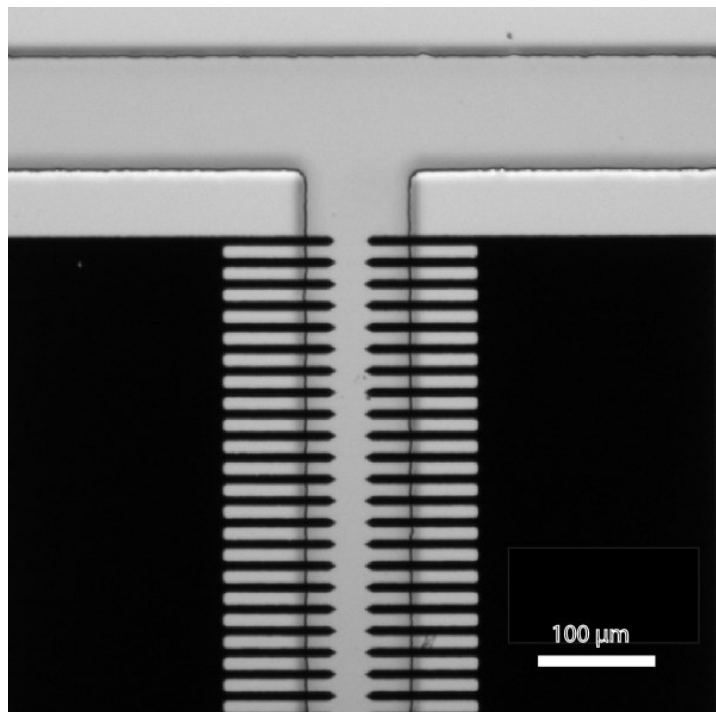


**Figure 4. Brightfield image of the inlet of the microfluidic T-channel with embedded electrodes<sup>12</sup>**



## 2.2 Chemical Solutions

### 2.21 Phosphate Buffer Solution and 6-Aminohexanoic Acid

Two fluid streams are introduced into the device via pressure driven flow from an externally pressurized cryogenic vial. Shown in Figure 5., the left-most (green) high conductivity stream consists of diluted 10X phosphate buffered saline (PBS) labeled with 10 ng/mL of Alexa Fluor 488 (Invitrogen). The right-most (red) high dielectric stream consists of 2M 6-aminohexanoic acid (Sigma-Aldrich) (AHA) labeled with 10 ng/mL of Alexa Fluor 594 (Invitrogen). AHA is a water-soluble zwitterion used for increasing the dielectric constant of aqueous solution. Prior to fluorescent labeling, the AHA solution is vigorously shaken for 5 minutes in 5 g/mL Dowex MR-3 (Sigma) ion exchange resin to remove trace salts and reduce solution conductivity.

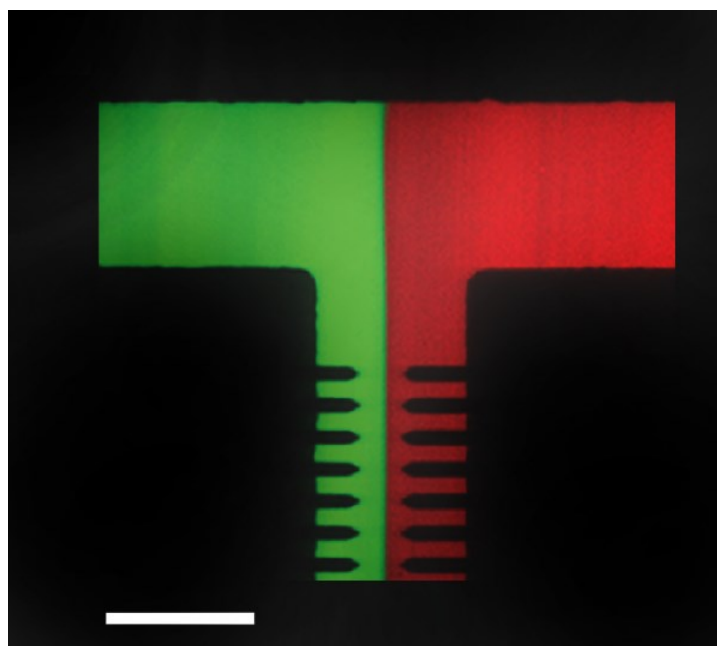


**Figure 5. Microfluidic T channel with embedded electrodes. Two fluid streams with different electrical properties— each imaged with a fluorescent dye—flow side by side to create an electrical interface.<sup>12</sup>**

### 2.2.2 Calcium Green-1

Calcium Chloride ( $\text{CaCl}_2$ ), Calcium Green-1 (CG1), Potassium Chloride (KCl) and 6-

aminohexanoic acid (AHA) were purchased from Sigma Aldrich. The CG1 was initially diluted to a 2 mM stock solution with DI water, then diluted down to a .2 mM stock solution with 2M 6-aminohexanoic acid and labeled with 10 ng/ml Alexa Fluor 405 (Invitrogen). The  $\text{CaCl}_2$  was diluted to 1 mM with DI water and labeled with 10 ng/ml Alexa Fluor 594 (Invitrogen). The resulting conductivities were 20  $\mu\text{S}/\text{cm}$  and .25 mS/cm respectively.<sup>13</sup>

### **2.2.3 Biotin and Avidin**

Biotin and avidin were purchased from Sigma Aldrich. The primary buffer, Buffer A, was made of 100mM NaCl, 50 mM  $\text{NaH}_2\text{PO}_4$  and 1 mM ethylenediaminetetraacetic acid (EDTA), pH adjusted to 7.5 with NaOH, all purchased from Sigma Aldrich. A biotin stock solution (4mM, 244.3 g/mol) was made with Buffer A. A standard solution (16  $\mu\text{M}$ ) was made by diluting the 4 mM stock with AHA and labeled with 10 ng/ml Alexa Fluor 594. Avidin solution (2.5  $\mu\text{M}$ , 66,000 g/mol) was made by adding 1.2 mg of pure avidin to 4 mL of Buffer A and labeled with 10 ng/ml Alexa Fluor 488. The concentration was calculated with a UV spectrometer. The UV was measured at  $A_{282}$  (per cm) and divided by the molar absorptivity of avidin ( $\epsilon_{282} = 96,000 \text{ M}/\text{cm}$ ).<sup>14</sup>

## **2.3 Pressure System**

Samples were delivered to the microfluidic device via a customized pressure system depicted below in Figure 6.

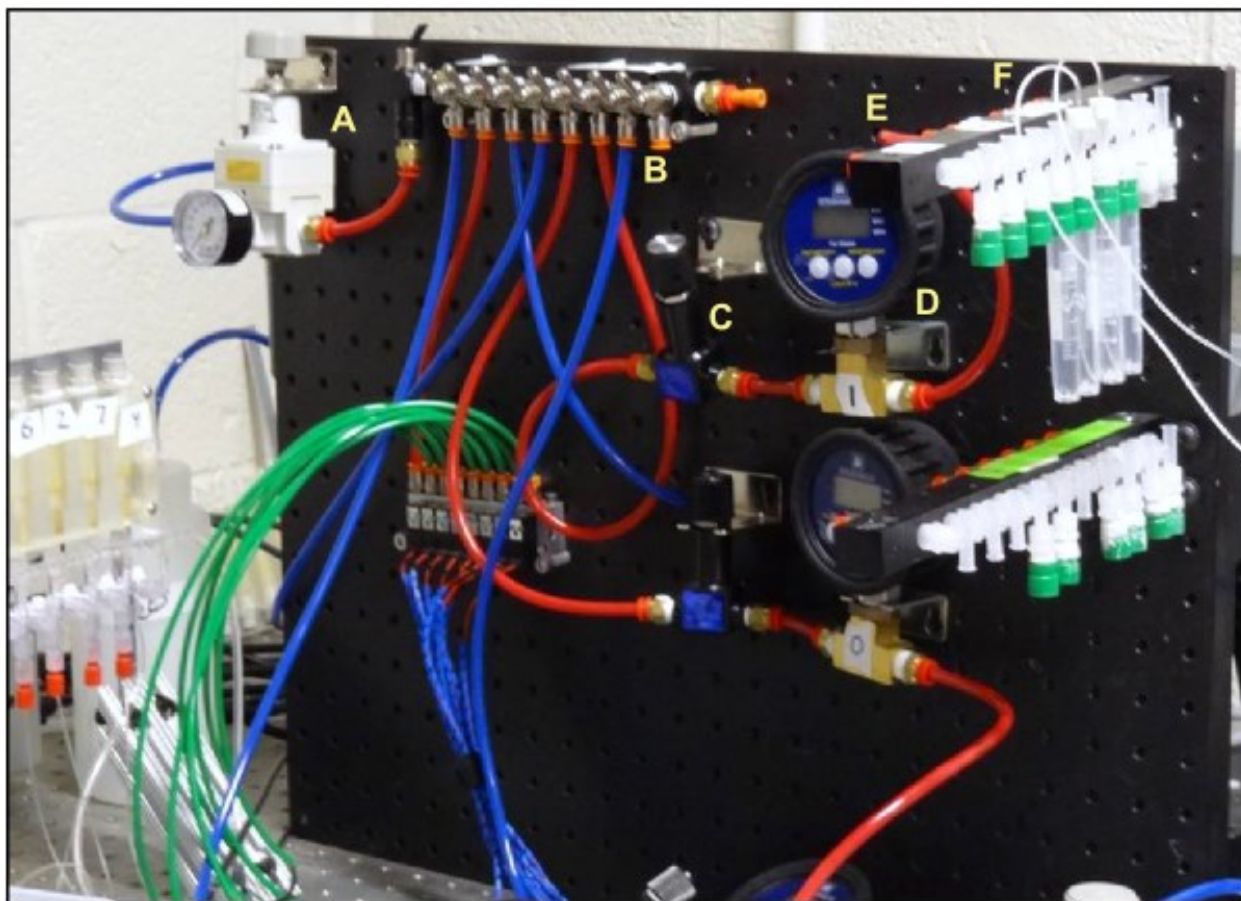


**Figure 6. Custom pressure system utilized for delivering samples to the microfluidic device**

Samples are loaded into 4-milliliter cryotubes, and delivered to the device by tubing. House gas is sent to a pressure regulator followed by a pressure gauge. From there, the gas is delivered to yet another pressure regulator and gauge (A), from which it is delivered to a series of outlet switches that deliver the gas to respective tubes (B). These outlet tubing, colored blue and red, are fed to another regulator and gauge, which is attached directly to cryotubes, (C), (D), and (E) respectively. The regulated house gas is fed through the side of the cryotube filling the tube with air. Since the cryotube is filled with sample, as the cryotube is pressurized, the sample needs to exit or the pressure will continue to build up. The sample exits out of the tubing which is

attached to the microfluidic device, delivering sample, (F). The pressure gauges (D) regulate the flowrates the samples are fed to the device.

## 2.4 Construction of a Microfluidic Liquid/Liquid Interface

Detection at the interface is based on an electrical-field induced fluid displacement of a liquid interface. This interface is created using two liquids of varying electrical properties - conductivity and permittivity – made to flow side-by-side during exposure to an ac electric field applied perpendicularly across the interface.

To create the electrical interface, two fluid streams, each with a different set of electrical properties, are pressure injected into the microfluidic device at a steady flow rate of 10  $\mu\text{L}/\text{min}$ . An AC potential of 10 volts peak-to-peak ( $V_{pp}$ ) at  $\omega = 1$  MHz is dropped across the electrodes and the frequency is slowly increased to 25 MHz while continuously monitoring the fluid interface. This was performed utilizing a Rigol DG4102 shown in Figure 7.<sup>15</sup>



**Figure 7: Rigol DG 4102 Function Generator used to deliver an electric field with varying frequencies and voltages across the liquid-liquid interface**

A cable is connected to the outlet port of the function generator at one end. The other end has two alligator clips; one active, the other is ground. Copper tape is attached to the pads, shown in

Figure 3, on the coverslip. Once the copper tape is applied to the chip, the alligator clips are attached to the copper tape. At this point, the voltage and frequency is selected on the function generator. Hitting the output button on the function generator delivers the electric field to the device, which is then applied across the liquid-liquid interface.

# Chapter 3

## Background

### 3.1 Maxwell-Wagner Polarization at Liquid-Liquid Interfaces

Since the embedded electrodes are on the bottom channel surface, fluid displacement is largely driven by polarization near the electrodes where the electric field ( $\mathbf{E}$ ) is largest. A charge neutrality condition at the liquid interface at the bottom channel surface will produce an observed crossover frequency, COF. across the entire electrical interface. The liquid interfacial COF is formulated for values of the electric field very near the substrate surface where it is assumed symmetric in the  $y$  direction (normal to the channel surface). Assuming each fluid is electroneutral, the electric potential in each phase very near the channel surface is well described by the one-dimensional Laplace equation in  $x$ ,

$$\frac{d^2 \phi_i}{dx^2} = 0 \quad \text{Equation 1}$$

where  $\Phi_i$  is the applied potential in the  $i$ th liquid stream, 1 (green) and 2 (red), and  $x$  points in the direction normal to the electric interface. We apply the usual MW boundary conditions at the electrical interface between the two liquid streams. First, as illustrated in Figure 8.<sup>12</sup>, we require the electric potential across the electrical interface ( $x = 0$ ) be continuous,  $\Phi_1(0) = \Phi_2(0)$ .

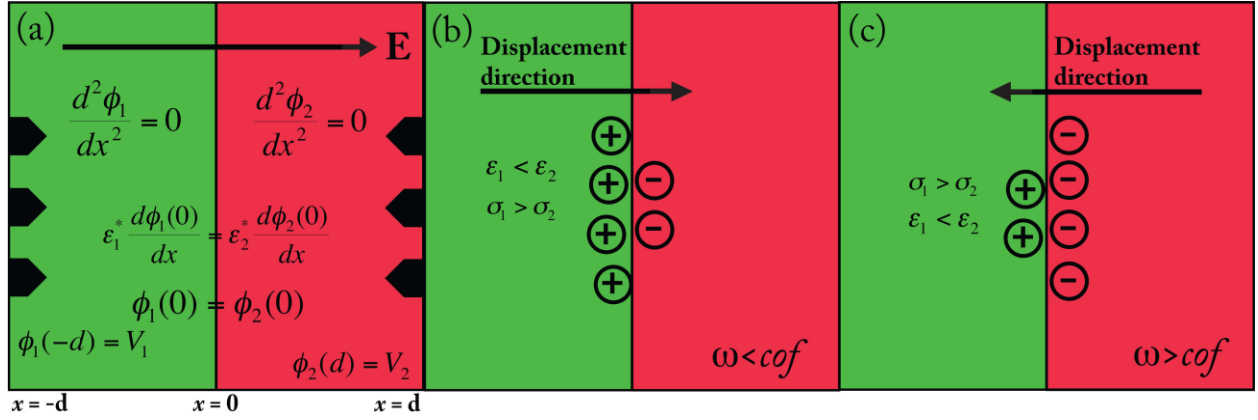


**Figure 8. Illustration of frequency-dependent MW polarization.**

Second, accounting for both Ohmic current (conductive polarization) and displacement current (dielectric polarization) across the interface, we require continuity in displacement current:

$$\varepsilon_1^* \frac{d\phi_1}{dx} - \varepsilon_2^* \frac{d\phi_2}{dx} = 0 \quad \text{Equation 2}$$

where

$$\varepsilon_i^* = \varepsilon_i - \frac{i\sigma_i}{\omega} \quad \text{Equation 3}$$

is the complex permittivity in each liquid phase. Hence, the fluid interface is subject to a net charge accumulation due to a discontinuous jump in conductivity and dielectric constant in order to satisfy the conservation of both ionic and dielectric charges. Using the above conditions, combined with boundary conditions for the applied potential,  $\Phi_1(-d) = V_1$ ,  $\Phi_2(d) = V_2$ , where  $V_1$  and  $V_2$  are the applied potential at each electrode ( $x = \pm d$ ), the Laplace equation in both liquid domains is solved. The interfacial COF occurs at an AC frequency where conductive charging completely balances dielectric polarization, and the net charge across the interface is zero. This condition occurs when the normal electric field ( $E_n = \frac{d\phi_1}{dx}$ ) is continuous across the liquid-liquid interface,

$$\frac{d\phi_1}{dx} - \frac{d\phi_2}{dx} = f = 0 \quad \text{Equation 4}$$

Based on the two-domain solution to the 1D Laplace equation, this liquid interfacial COF occurs when  $f(\omega) = \frac{\varepsilon_1^* - \varepsilon_2^*}{\varepsilon_1^* + \varepsilon_2^*} = 0$ . It is important to note that  $f(\omega)$  is a complex function, and has both real (in-phase with the applied field) and imaginary (out of phase) parts. The electric field is applied as a single sinusoid, so there is no phase gradient, and charging is driven by the in-phase component (real part) of the electric field. Thus, the predicted crossover frequency ( $\omega_{co}$ ) where induced interfacial charge vanishes is determined by  $\text{Re}[f(\omega)] = 0$ , or in functional form,

$$\omega_{co} = \frac{1}{2\pi} \frac{(\sigma_1 - \sigma_2)(\sigma_1 + \sigma_2)^{1/2}}{(\varepsilon_2 - \varepsilon_1)(\varepsilon_2 + \varepsilon_1)^{1/2}} \quad \text{Equation 5}$$

### 3.2 Calcium Green-1

Calcium Green-1 (CG1) is a chemical indicator that chelates calcium ions. Calcium Green-1 is based on an EGTA homologue called BAPTA. BAPTA is a calcium-specific aminopolycarboxylic acid. Due to the presence of four carboxylic acid functional groups, BAPTA can bind to two calcium ions. Calcium Green-1 is generally used to measure intracellular  $\text{Ca}^{2+}$ , following  $\text{Ca}^{2+}$  influx and release, and excitation imaging of  $\text{Ca}^{2+}$  in living tissues.<sup>16</sup> CG1 shows a 14-fold increase in fluorescent intensity when chelating  $\text{Ca}^{2+}$ . CG1 is shown in Figure 9 below.<sup>17</sup>



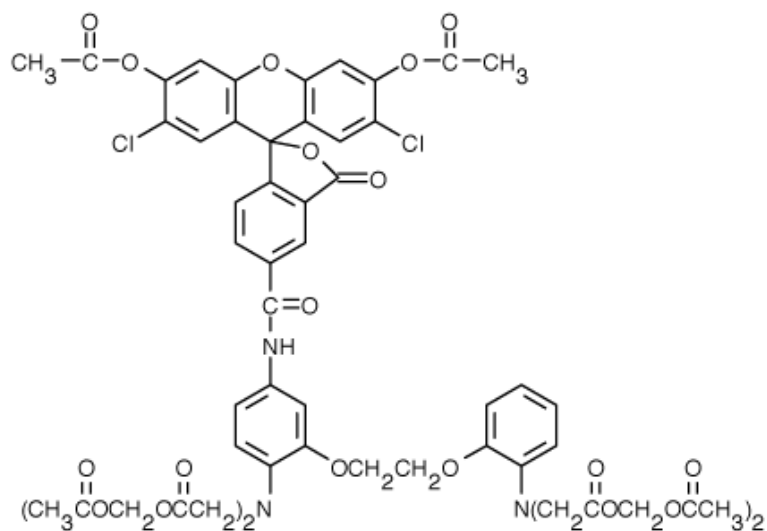


**Figure 9. Calcium Green-1 Structure**

### 3.3 Biotin and Avidin

Biotin, also known as vitamin H, is a small molecule present in all living cells. Generally present in small amounts, it is critical for many biological processes. The valeric acid side chain, seen on the biotin molecule in Figure 10<sup>18</sup>, can be derivatized to attach other reactive groups used to bind biotin to other molecules. Generally, biotin is conjugated to antibodies or enzyme reporters used to detect target antigens.

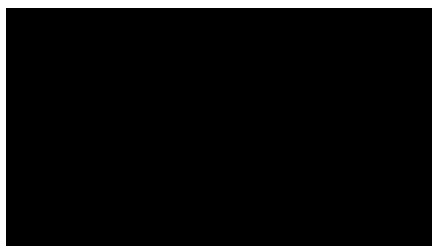


**Figure 10. Biotin Structure**

Due to the large binding affinity of avidin to biotin, any biotin-containing molecules in a complex mixture can specifically bind to avidin. Avidin is a glycoprotein found in egg whites and tissues of birds, reptiles, and amphibia. Avidin contains four identical subunits and has a mass of roughly 66 to 68 kDa. Each subunit can bind to one biotin molecule; thus, a total of four biotin molecules can bind to a single avidin molecule. The avidin-biotin binding complex is the strongest known non-covalent interaction between a protein and a ligand. This bond formation is extremely rapid, and once formed, is unaffected by pH, temperature, organic solvents, and other deterring agents. These factors alone make the Avidin-Biotin binding complex optimal for biomedical applications.<sup>19</sup>

# Chapter 4

## Results and Discussion

### 4.1 Fluidic Dielectrophoresis

Two streams of varying electrochemical properties flow side-by-side to create a liquid-liquid interface within the T-channel device. The varying electrochemical properties are conductivity and permittivity. One stream, PBS, has a high conductivity (.29 mS/cm) but a low permittivity ( $\epsilon = 80$ ). The other fluid, AHA, has a low conductivity (19  $\mu$ S/cm) but a high permittivity ( $\epsilon = 110$ ). Due to the difference in conductivity and permittivity, the two streams undergo interfacial polarization as well as liquid displacement. When an electric field is applied perpendicularly to the interface at low frequencies (1 MHz) the liquid with the higher conductivity displaces into the liquid with the lower conductivity. When an electric field with a high frequency (20 MHz) is applied the liquid with the high permittivity displaces into the liquid with the lower permittivity. The frequency at which no displacement occurs is known as the COF. This phenomena is illustrated below in Figure 11.<sup>12</sup>

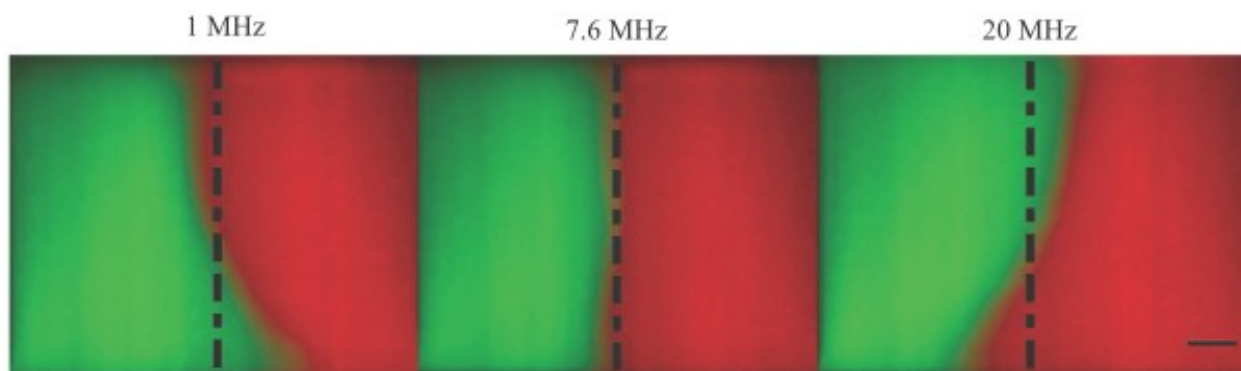


**Figure 11. Confocal cross section of the interface**

Given the original conditions, the COF was found to be 7.6 MHz. From here, the electrochemical influence was studied. The conductivity differences were studied and the influences were

compared with theoretical values. At low frequency, below the inverse charge relaxation time, the high-conductivity stream conducts ionic charge to the interface at a rate faster than can be removed by the adjacent low-conductivity liquid. As such, the high-conductivity fluid dominates the polarization of the interface. At high frequency, when ionic charging does not have enough time to occur, the high-dielectric liquid governs the interfacial charging. Therefore, the net sign of the induced interfacial charge between the two liquids reverses depending upon the ac frequency applied, since neither liquid has both greater conductivity and dielectric constant. As charge reversal can occur, there exists an intermediate frequency where conductive charging is equally balanced by dielectric charging, and the interface has a zero net charge. The observed increase in COF with increasing differences in electrical conductivity is consistent with this argument shown below in Figure 12.<sup>12</sup>

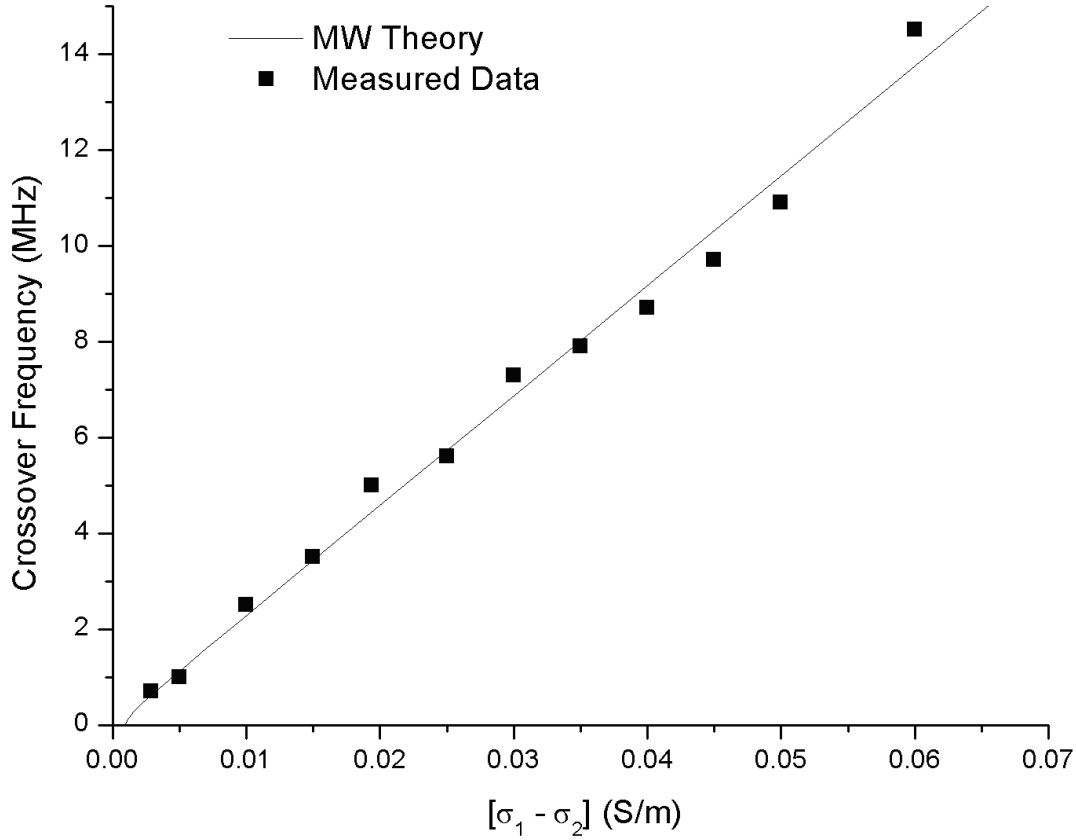


**Figure 12. Comparison between experimental (symbols) and analytical (line) interfacial COF as a function of the difference in electrical conductivity between each fluid stream,  $[\sigma_1 - \sigma_2]$ . Error bars are of the order of the size of symbols.**

The theoretical line was graphed using Matlab, the code can be found in Appendix A. After quantifying the influence of conductivity differences between streams, permittivity differences were evaluated. While increasing conductivity differences leads to an increase in the COF, there is an opposite affect with permittivity. When the difference in permittivity decreases, the COF of the system increases. If we reference Equation 5, we can see that this holds true since permittivity values are in the denominator of the equation, leading to a reciprocal effect. This is illustrated in Figure 13. The theoretical line was created using the Matlab code in Appendix A, but instead of inputting a delta sigma, a delta epsilon was plotted.

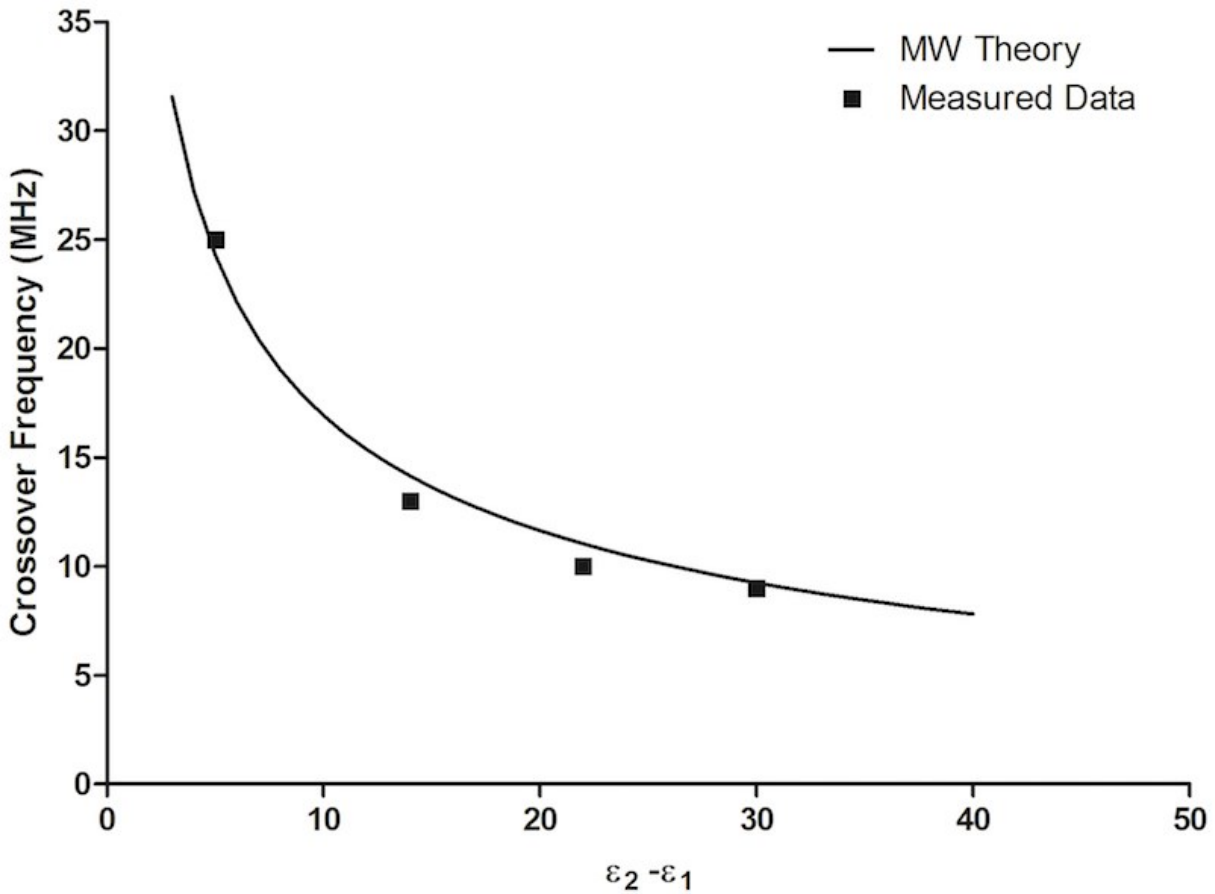


Figure 13. Comparison between experimental (symbols) and analytical (line) interfacial COF as a function of the difference in electrical conductivity between each fluid stream,  $[\sigma_1 - \sigma_2]$ . Error bars are of the order of the size of symbols.

## 4.2 Calcium Detection

The next experiment proved liquid-liquid interfacial detection was possible by using a well-known chelator, calcium green, CG1. CG1 was chosen for two main reasons: 1) CG1 has a high binding affinity for  $\text{Ca}^{2+}$  and 2) when binding occurs, the complex fluoresces with a 14-fold intensity. This increase in fluorescence indicates the reaction is occurring downstream on the chip. A Dextran bound CG1 molecule was selected for several significant reasons but mainly to make the system diffusing limited. The concentration of calcium green at the interface was kept fairly constant during a constant flux of calcium ions. Secondly, having the CG1 bound to a

dextran molecule made for a perfect control experiment. Running the experiment with a dextran molecule of the same molecular weight revealed whether the reaction was detected by the system eliminating any concern of diffusional effects. Finally, the CG1 bound to dextran gives way to more analysis on diffusional effects later on when altering the molecular weight of the dextran molecule bound to the calcium green.

The experiment began by flowing two streams side by side down the T-channel: .2mM CG1 with 10ng/ml Alexa Fluor 405 and 1mM  $\text{Ca}^{2+}$  with 10 ng/ml Alexa Fluor 594 (Figure 14.). A saturated reaction scheme was chosen with  $\text{Ca}^{2+}$  because it diffuses across the interface at a fast rate ensuring the system was not reaction limited, but rather diffusion limited. Two fluids, one with calcium green-1 and the other with  $\text{CaCl}_2$ , flowed side by side down a microfluidic T-channel device with integrated electrodes, as shown in Figure 14. The two streams were dyed separate colors, the CG1 stream was purple and the  $\text{CaCl}_2$  was red. When the calcium was chelated by the CG1 it fluoresced with a greater intensity than the CG1 stream alone, which became white with a green tint. This fluorescence intensity was shown at the interface down the axial length of the channel. An alternating current was applied perpendicular to the interface and the interfacial response studied.

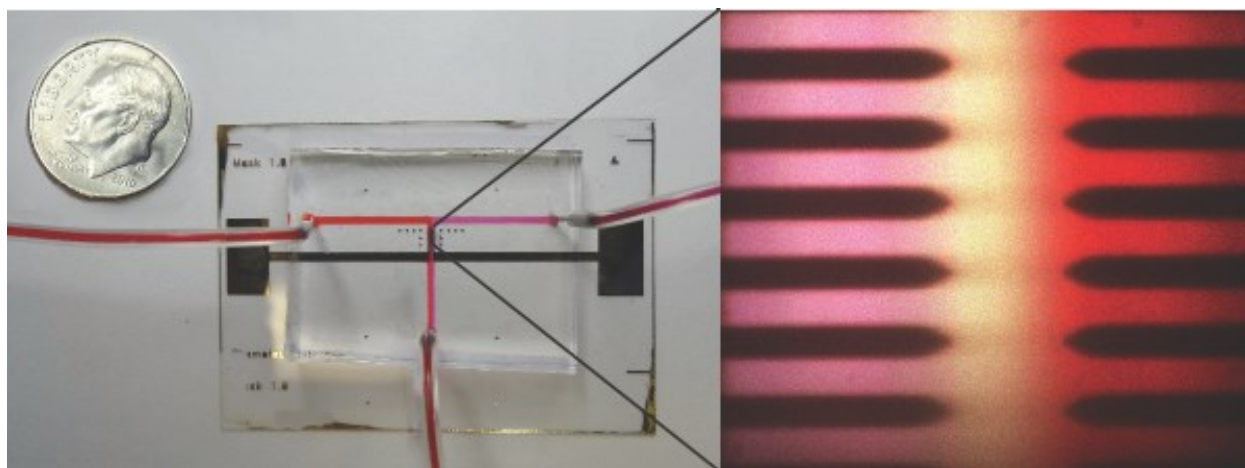


**Figure 14. Microfluidic T-channel zoomed in on the interface**

At low frequencies the high conductive stream deflected into the low conductive stream, while at high frequencies the deflection reversed. There was a frequency at which no deflection occurred, known as the crossover frequency (COF). This phenomenon is shown in Figure 15. with the product shown at the interface.

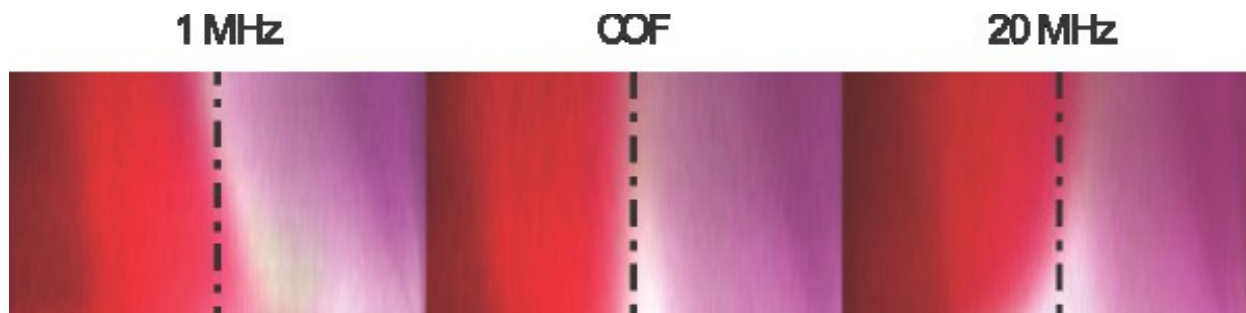


**Figure 15. Confocal cross section of the interface. Reaction between CG1 and  $\text{Ca}^{2+}$  occurring at the interface**

By measuring the COF changed down the axial length of the stream, it was determined the COF of the system increased as shown in Figure 16. This COF change was plotted against the theoretical COF based on the concentration of product and reactants down the axial length of the channel shown below.



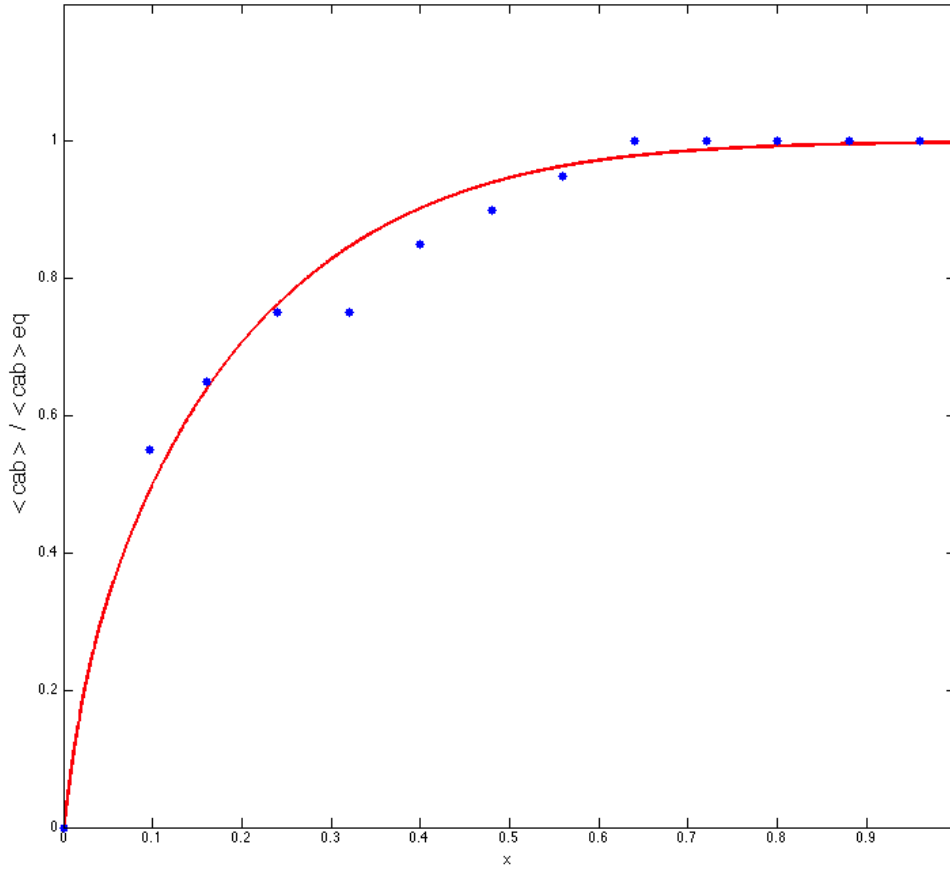


**Figure 16. Comparison between experimental (symbol) and theoretical (line) COF down the axial length of the channel**

The code for this plot can be found in Appendix B. The change in COF indicates an electrochemical change occurs at the interface. This change can be accredited to the conductivity at the interface decreasing down the axial length of the channel. While the conductivity of the  $\text{Ca}^{2+}$  stream remains the same, in order for the COF to increase, the conductivity of the adjacent stream must decrease. The measured COF of a system is linearly related to the change in conductivity between the two liquid streams. Since the COF increased down the channel, the conductivity decreased as more product formed .

This alone was not enough to prove that product detection was occurring; there could have been other reactions giving rise to a COF change (i.e. nonspecific reactions). Running a series of control experiments eliminated doubt, shown in Figure 17.

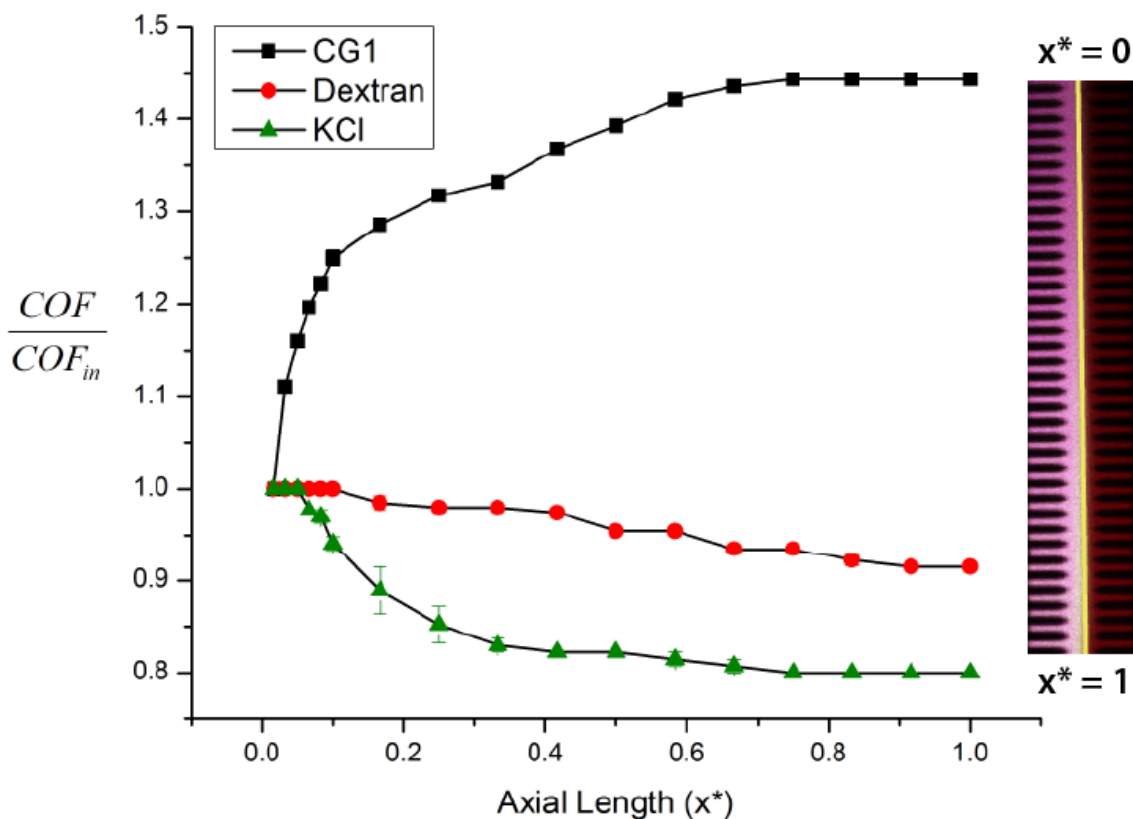


**Figure 17.** Calculated COF down the axial length of the channel for CG1, Dextran (positive control), and KCl (negative control)

The first control was a fluorescently tagged dextran molecule with the same molecular weight as CG1 bound to dextran; this was to –eliminate? altered results due to changes in diffusional properties. When the two streams,  $Ca^{2+}$  and Dextran, flowed side-by-side, a decrease in the COF down the axial length of the channel was observed, as illustrated in Figure 17. This

shows that while moving axially down the channel, an electrochemical change of the interface was occurring due to dilution, not a reaction. A control with CG1 was now needed to prove this method fully. For this purpose, potassium chloride (KCL) was run side-by-side with CG1; a larger molecule that will not fit in the CG1 binding site. Once again decrease in COF was observed (Figure 17) illustrating no reaction was present and further indicating product formation was detected by means of the COF. It is interesting to see that the rate of COF decrease is different between the two controls. This is due to diffusional differences between the two molecules. The molecular weight of the dextran used was 3000 g/mol while the molecular weight of KCl is 74.55 g/mol. Since the KCl can diffuse faster than the dextran, in its respective system, the COF change is more drastic. Thus, this method of detection at a liquid-liquid interface can also be used for ion detection. Now, the next step is to determine if this method could be used as a biosensor to detect specific protein interactions at an interface.

### **4.3 Avidin-Biotin Reaction**

Avidin was chosen as the protein of choice for studying the COF of the interaction because of its high specificity and affinity for the biotin-avidin reaction. Two streams flowed side-by-side, much like the CG1 experiment, one containing Avidin the other Biotin. The same experiment was performed as previously with the CG1, studying the COF changes down the axial length of the channel. A series of three experiments were run to prove this method of detection was valid: Avidin/Biotin, Biotin/Buffer A, and Avidin/AHA. The last two experiments were used as controls to determine if any electrochemical changes at the interface in the first experiment were due to product formation.

Like the CG1 experiments, avidin and biotin streams flowed side-by-side down the channel and the COF was calculated. It was found that while moving down the length of the channel, the COF of the system increases as shown in Figure 18.

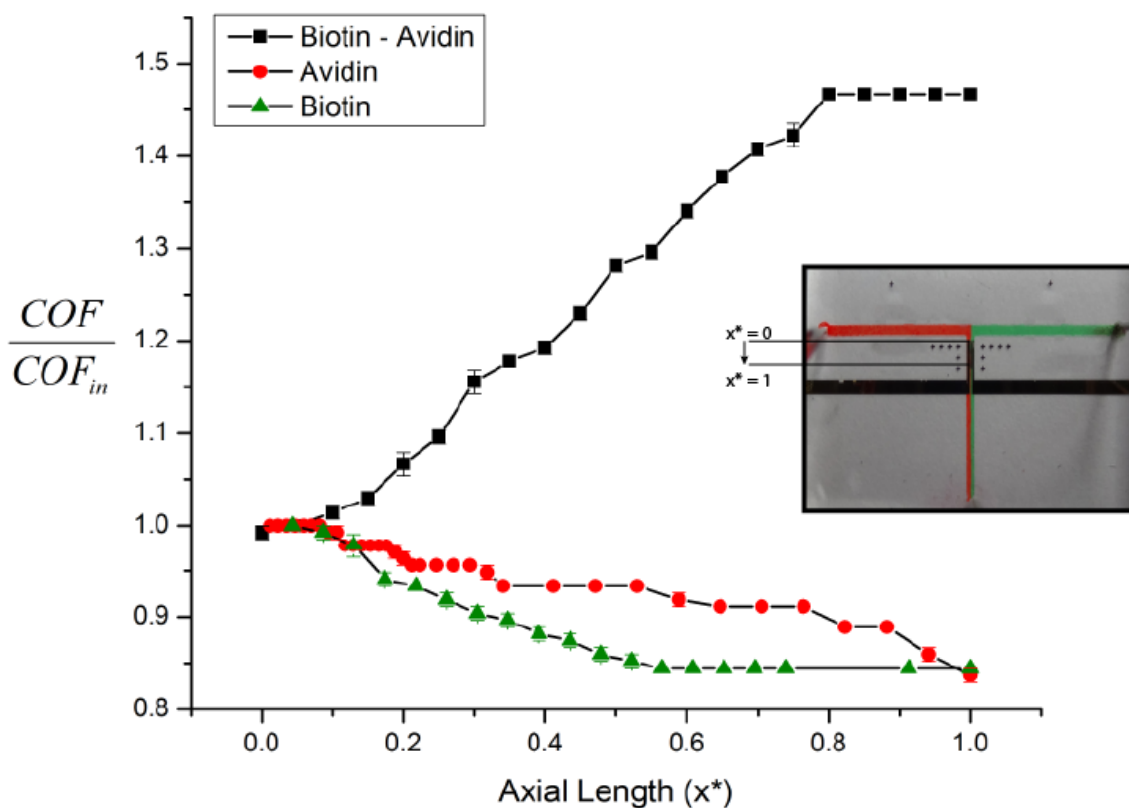


**Figure 18. Calculated COF down the axial length of the channel for Biotin-Avidin, Avidin-AHA (control), and Biotin-Buffer A (control)**

Since the COF increases, it can be concluded that the conductivity at the interface is decreasing due to the Biotin-Avidin product formation. This demonstrates the presence of product is detected by means of the COF. As further proof, two control experiments were conducted: Avidin/AHA and Biotin/Buffer A. When the COF was determined for each run, it

was found that when moving down the axial length of the channel, the COF decreases. This decrease is the result of dilution at the interface due to diffusion. Additionally, the rate of COF decrease was found to be different between the two control systems. This further solidifies that diffusion was the contributing factor in the COF change. Biotin has a molecular weight of 244 Daltons while avidin has a molecular weight of 66,000 Daltons. As a result of the difference in molecular weight, the diffusion rates of the two molecules are significantly different. This explains why the COF in the biotin control experiment decreased more rapidly than the COF in the avidin control, further proving detection and presence of product formation in the previous experiment where COF increased vs. the latter experiment where COF decreased when one of the reactants was not present in both systems.

These experiments were run at varying flow rates to determine how the COF values change with time. This system was run at 4, 6.5, 8.75, and 10  $\mu\text{L}/\text{min}$ ; the varying COF was calculated down the channel, shown in Figure 19.

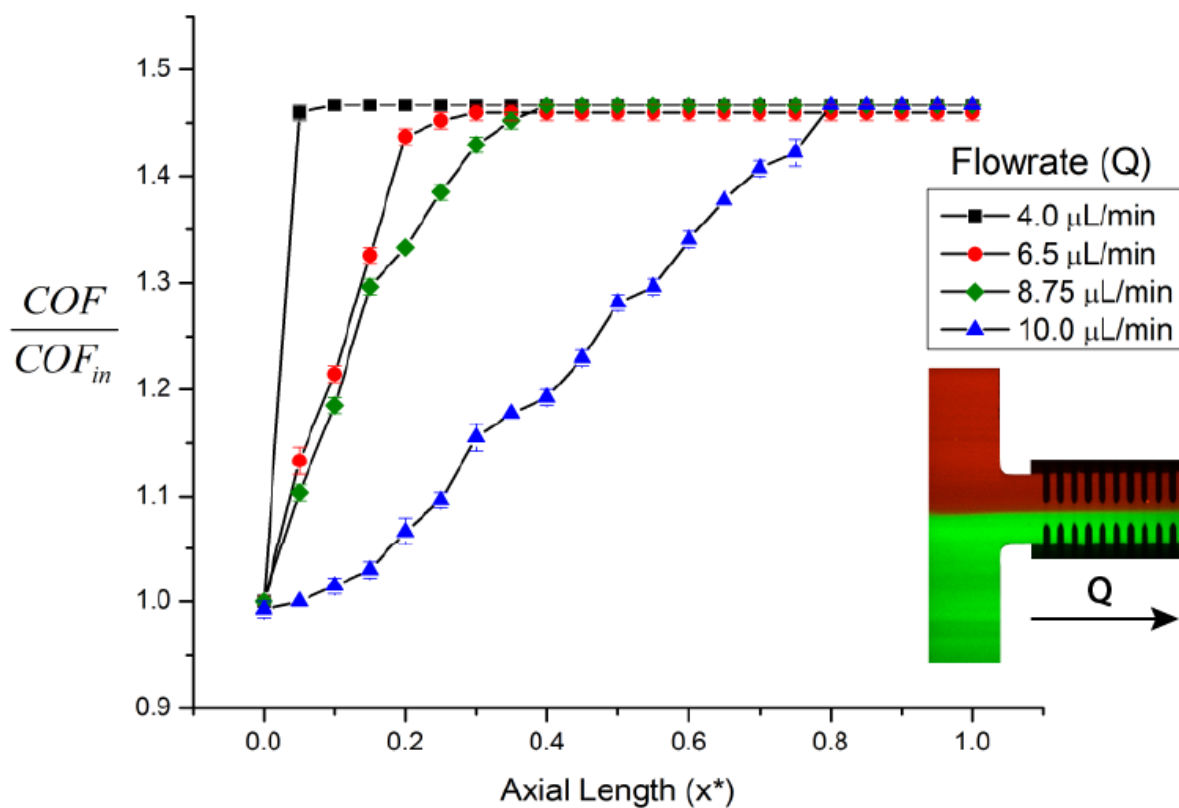


Figure 19. Calculated COF down the axial length of the channel at varying flowrates

At slower flow rates the system reaches equilibrium much faster since slower flow rates allow for the reaction to occur over a greater time scale. This also implies this method can be used to measure immediate product formation.

# Chapter 5

## Conclusion and Future Work

In conclusion, a highly sensitive biosensor was developed utilizing a liquid-liquid interface. Initially, the effects of disparaging electrochemical properties, conductivity and permittivity, were quantified. Next, ions were detected within the microfluidic system by chelating  $\text{Ca}^{2+}$  with CG1. The system was then utilized to detect avidin with a biotin reaction. It was observed that as the  $\Delta\sigma$  increases, the measured COF increases. A reciprocal effect was found with permittivity, as the  $\Delta\epsilon$  decreases, the measured COF increases. Next, it was observed as product forms at the interface, the electrochemical properties of the interface change. The conductivity at the interface decreases leading to an increase in the change in conductivity. This increase leads to a rise in the COF down the axial length of the channel.

In the future, experiments will be conducted to determine how diffusional effects can vary the change in the COF. There will be experiments to correlate the magnitude of the COF directly with the concentration of product formed. Lastly, we must detect more physiological relevant substrates and use this for more diagnostic applications such as to determine if certain proteins are present in cancer or HIV patients, foe example. Finally, scientists can use this method as a multiplexing system. Each reaction will yield a different COF once it has reached equilibrium, how ever small these variations may be. This property can be utilized and apply varying COF downstream to determine if certain proteins of interest are present amongst a variety of proteins in your system.

Utilizing interfacial polarization and frequency-dependent displacement at a liquid-liquid interface in a lab-on-a-chip device has many benefits over current methods. This paper describes the creation of a liquid-liquid substrate by which the reaction can occur and be studied.

Furthermore, because the transducer is the liquid-liquid interface and the interface is where the reaction occurs, this method eliminates nonspecific binding. Another interesting characteristic is that at any given position along the liquid-liquid interface, the resulting reaction occurring is continuous. As reactions occur, reactants move along the channel, react, and are replaced with new reactants, allowing for the same reaction to occur over and over. This enables the study and alteration of a specific point on the reaction kinetic scheme. Finally, this method facilitates portability. The device is compact, roughly the size of a quarter and as a result, requires a minimal volume of materials, on the order of microliters.



## References

1. Dancil, K. P. S., Greiner, D. P., & Sailor, M. J. (1999). A porous silicon optical biosensor: detection of reversible binding of IgG to a protein A-modified surface. *Journal of the American Chemical Society*, 121(34), 7925-7930.
2. Yemini, M., Reches, M., Gazit, E., & Rishpon, J. (2005). Peptide nanotube-modified electrodes for enzyme-biosensor applications. *Analytical Chemistry*, 77(16), 5155-5159.
3. Millan, K. M., Saraullo, A., & Mikkelsen, S. R. (1994). Voltammetric DNA biosensor for cystic fibrosis based on a modified carbon paste electrode. *Analytical chemistry*, 66(18), 2943-2948.
4. Nguyen, T. A., Yin, T. I., Reyes, D., & Urban, G. A. (2013). Microfluidic chip with integrated electrical cell-impedance sensing for monitoring single cancer cell migration in three-dimensional matrixes. *Analytical chemistry*, 85(22), 11068-11076.
5. Hansen, J. A., Wang, J., Kawde, A. N., Xiang, Y., Gothelf, K. V., & Collins, G. (2006). Quantum-dot/aptamer-based ultrasensitive multi-analyte electrochemical biosensor. *Journal of the American Chemical Society*, 128(7), 2228-2229.
6. Haes, A. J., & Van Duyne, R. P. (2004). A unified view of propagating and localized surface plasmon resonance biosensors. *Analytical and Bioanalytical Chemistry*, 379(7-8), 920-930.
7. Zhang, Y., & Tadiadapa, S. (2004). Calorimetric biosensors with integrated microfluidic channels. *Biosensors and Bioelectronics*, 19(12), 1733-1743.
8. Andle, J. C., & Vetelino, J. F. (1994). Acoustic wave biosensors. *Sensors and Actuators A: Physical*, 44(3), 167-176.
9. Pattnaik, P. (2005). Surface plasmon resonance. *Applied biochemistry and biotechnology*, 126(2), 79-92.
10. Long, D. A., & Long, D. A. (1977). *Raman spectroscopy* (Vol. 206). New York: McGraw-Hill.
11. Wu, G., & Zaman, M. H. (2012). Low-cost tools for diagnosing and monitoring HIV infection in low-resource settings. *Bulletin of the World Health Organization*, 90(12), 914-920.
12. Desmond, M., Mavrogiannis, N., & Gagnon, Z. (2012). Maxwell-Wagner Polarization and Frequency-Dependent Injection at Aqueous Electrical Interfaces. *Physical review letters*, 109(18), 187602.
13. Baroud, C. N., Okkels, F., Ménétrier, L., & Tabeling, P. (2003). Reaction-diffusion dynamics: confrontation between theory and experiment in a microfluidic reactor. *Physical Review E*, 67(6), 060104.
14. Ebner, A., Marek, M., Kaiser, K., Kada, G., Hahn, C. D., Lackner, B., & Gruber, H. J. (2008). Application of biotin-4-fluorescein in homogeneous fluorescence assays for avidin, streptavidin, and biotin or biotin derivatives. In *Avidin-Biotin Interactions* (pp. 73-88). Humana Press.

15. Rigol. *DG4102 | 100 MHz Arbitrary Waveform Generator*. Retrieved from <http://www.rigolna.com/products/waveform-generators/dg4102/>
16. Molecular Probes. *Calcium Green<sup>TM</sup>-1 dextran, Potassium Salt, 3000 MW, Anionic*. Retrieved from <https://www.lifetechnologies.com/order/catalog/product/C6765?ICID=search-product>
17. Fluorophores. *Calcium Green-1*. Retrieved from <http://www.fluorophores.tugraz.at/substance/646>
18. Biochemistry and Computer Science. *Drawing Coenzymes Structures*. Retrieved from [http://www.biochemcs.com/coenzymes\\_structures.htm](http://www.biochemcs.com/coenzymes_structures.htm)
19. Sinder, J. *Avidin-Biotin Complex Method for IHC Detection*. Retrieved from <http://www.piercenet.com/method/avidin-biotin-complex-ihc-detection>

# Appendix

## Appendix A: Theoretical Crossover Frequency Matlab Code

```
clc;
clear all;

splist = logspace(-6,-1,40)

for i = 1:40
    sp=splist(i);

e0 = 8.85e-12;
sm = 0.001; %AHA conductivity
em = 110*e0; %AHA perm
%sp = 0.02; %high conductive PBS
ep = 78.2*e0; %perm of PBS
f = logspace(4,10,1000);
w = 2*pi*f;
j = sqrt(-1);
epc = (ep-j*sp./w);
emc = (em-j*sm./w);
cm = (epc-emc)./(epc+emc);
output = real (cm);
%semilogx(f,output);
xlabel('Frequency (Hz)');
ylabel('Re[k(w)]');

%root solver
marker = 0;
for k = 1:1000
    if output(k)>0
        marker = k;
    end
end
if marker<1000
    if marker>0
        xlower = f(marker);
        vlower = output(marker);
        xupper = f(marker+1);
        vupper = output(marker+1);
        ratio = vupper/(vlower-vupper);
        crossover = xlower+ratio*(xupper-xlower);
    else crossover = 0.01;
    end
else crossover = NaN;
end

crossoverlist(i) = crossover;
end;
plot((splist-sm),crossoverlist);
xlabel ('Conductivity (Sm-1)');
ylabel('Crossover Frequency (Hz)');
%axis([1e-3 1e-1 1e5 1e7]);
hold on
```

```
data_cond = [0.0194 0.016 0.01 0.005 0.0029 0.051 0.046 0.041 0.036 0.031  
0.026 0.061]  
  
data_crossover = [5e6 3.5e6 2.5e6 1e6 0.7e6 10.9e6 9.7e6 8.7e6 7.9e6 7.3e6  
5.6e6 14.5e6]  
  
plot((data_cond - sm),data_crossover,'*');
```

## Appendix B: Theoretical Crossover Frequency for Concentration of Product Matlab Code

```
clc;
clear;

delta = 0.5;
tol = 0.00001;
del = 0.5;

l=1; %aspect ratio

count = 0;

a = 0.01;
m=0.01;
n=100;

while count < n
    count=count+1;
    b=a+delta;
    fa=cos(a);
    fb=cos(b);

    while fa*fb>0

        a=b;
        b=b+del;

        fa=cos(a);
        fb=cos(b);

    end
    fm=1;
    while abs(fm)>tol;
        m = (a+b)/2;
        fm = cos(m);

        if fa*fm<0;
            b=m;
            fb=fm;
        else
            a=m;
            fa=cos(m);
        end
    end
    xm(count)=m;
    a=m+del;
end

for y=.106
```

```

counter=0;

for x=0:.001:1
    counter=counter+1;
    xx(counter)=x;

    sum=0;

    for i=1:n

        A(i)=(2/(xm(i)));

        sum=sum+A(i)*exp(-(xm(i)^2)*x)*sin(xm(i)*y);

        u(counter)=sum;

    end

end

end

plot(xx,u,'LineWidth',1.2,'Color','g');
hold on
%plot(xx,ushear);
xlabel('X*');
ylabel('Dimensionless Concentration');
end

```

# Curriculum Vitae

## EDUCATION

**Johns Hopkins University**, Baltimore, Maryland  
May 2014  
Major: *Chemical and Biomolecular Engineering Masters of Science*  
Concentration: Biochemical Engineering  
Expected Graduation: May 2014

**Johns Hopkins University**, Baltimore, Maryland  
May 2013  
Major: *Chemical and Biomolecular Engineering Bachelors of Science*  
Concentration: Bioengineering

## WORK EXPERIENCE

**Zachary Gagnon Lab**, Baltimore, MD  
*Research Assistant*  
January 2012 - Present

- Fabrication in class 1000 clean room with positive and negative photolithography
- Design and printing of microfluidic devices with AutoCAD, with translation to postscript
- Operation of Nikon confocal and TIRF microscope with NIS Elements software
- Study interfacial properties of immiscible and miscible fluids when an electric field is induced.

**GE Healthcare**, Piscataway, New Jersey  
*Bioprocess Chromatography Engineer*  
Summer 2011

- Developed Pressure-Flow curves and resin integrity tests for Capto SR ImpRes resin packed in Axichrom 100 chromatography columns. This data is used to determine optimal packing parameters for the chromatography media/column combination. The data is logged in a company wide library database for GEHC Customer Support personnel.

**GE Healthcare**, Piscataway, New Jersey  
*Bioprocess Chromatography Engineer*  
Summer 2010

- Developed Van Deemter and Pressure-Flow curves for GEHC Sepharose IEX resin packed in BPG 100 and 200 chromatography columns. This data is used to determine optimal packing parameters for the chromatography media/column combination. The data is logged in a company wide library database for GEHC Customer Support personnel.

## PUBLICATIONS

- **"Maxwell-Wagner Polarization and Frequency Dependent Injection at Aqueous Electrical Interfaces"** by Mitchell Desmond, Nicholas Mavrogiannis, and Zachary Gagnon  
*Physical Review Letters*. In press October 2012.

## AWARDS

- Chemical and Biomolecular Engineering Undergraduate Research Award
- Chemical and Biomolecular Engineering Excellence Member